Materials for Renewable and Sustainable Energy (2025) 14:25
https://doi.org/10.1007/s40243-025-00299-6

ORIGINAL PAPER

Evaluating thermal storage capability of recycled construction materials: an experimental approach

Fardin Jafari[1] · Giovanni Semprini[2] · Alessandra Bonoli[1]

Received: 30 September 2024 / Accepted: 11 February 2025

Abstract

Granular materials like sand have gained importance in thermal storage applications due to their stability and cost-effectiveness. However, excessive usage of sand can pose environmental issues. This study investigates recycled construction materials such as glass, asphalt, ceramic, and concrete as alternatives to natural sand for low-temperature TES applications. The materials were processed to similar grain sizes and evaluated for their chemical, thermophysical, and thermal storage properties through a six-hour charging cycle at 60 °C. XRF analysis revealed significant compositions, including high oxygen and silicon content in concrete and sand, respectively. Results indicate that sand with 0.189 W/m K recorded the highest thermal conductivity compared with concrete 0.172 W/m K, glass 0.131 W/m K, ceramic 0.159 W/m K and asphalt 0.159 W/m K. A higher specific heat capacity was observed in concrete at 755 J/kg K, followed by asphalt at 732 J/kg K, glass at 708 J/kg K, and sand at 688 J/kg K. However, ceramic is categorized for a lower specific heat capacity of 682 J/kg K. Absolute density evaluation indicates that sand is the densest material with 2662 kg/m^3, contrary to concrete 2480 kg/m^3, glass 2421 kg/m^3, ceramic 2285 kg/m^3, and asphalt 2436 kg/m^3. More to the point, the Ragone plot for specific power and energy highlighted that ceramic has a rapid energy release and concrete demonstrated sustained energy storage capabilities. Volumetric power and energy density assessments indicated sand's outstanding performance. However, concrete registered a superior thermal storage among recycled materials. The results highlight that recycled materials, specifically concrete can be used for thermal storage applications like water heating in poor communities.

Keywords Thermal storage · Recycled materials · Ragone plot · Thermal conductivity · Specific heat capacity

Introduction

Thermal energy storage has increasingly gained importance in modern energy management and has become a key factor in conserving renewable energy, like solar or wind [1–3]. One of the major challenges in the building and residential sectors is reaching nZEB or ZEB targets, where energy needs, especially those for heating and domestic hot water, must be completely supplied by renewable sources. Due to the different time profiles of users' energy consumption and energy production from renewable sources, it is necessary to provide energy storage. Therefore, the produced energy can properly be stored and supplied to the building technical systems at the requested time [4–6]. Using lithium-ion batteries to store electricity from renewable sources imposes significant costs for their provision and maintenance, and they also have a short lifespan so thermal energy storage can be a suitable option instead of batteries [7–9]. Instead, the thermal energy can be stored in more sustainable and cheaper systems through various materials and in different physical states, like solid, molten, and liquid phases [10, 11]. TES performance relies heavily on key thermal properties of materials, such as thermal conductivity and specific heat capacity, which determine their efficiency in storing and releasing energy. Materials with higher thermal conductivity facilitate efficient heat transfer, while those with higher specific heat capacity store larger quantities of energy. Thermal oils and liquid sodium are liquid TES materials often used for storage and heat exchanger fluid because

✉ Fardin Jafari
Fardin.Jafari2@unibo.it

[1] Department of Civil, Chemical, Environmental and Materials Engineering, University of Bologna, Bologna, Italy

[2] Department of Industrial Engineering, University of Bologna, Bologna, Italy

Published online: 04 March 2025

they have high thermal conductivity [12, 13]. Materials like molten salts and metals are considered thermal storage materials for solar energy concentration. However, keeping molten materials at a constant temperature is crucial to their application to achieve optimum efficiency since overheating can reduce their efficiency[14–16].

Meanwhile, molten state TES can damage the storage vessel and piping networks due to solidification[17]. Metals can also cause corrosion inside the storage tank, so specific materials are required and associated additional costs [18]. One of the TES materials of interest in solid-state is sand, which offers higher thermal tolerance with a melting point of 1700 °C [19, 20]. Additionally, sand provides notable cycle stability over time, making it a reliable material to store thermal energy [21–23]. Therefore, sand has gained considerable attention in designing thermal storage systems.

Various studies have been developed to optimize sand performance in thermal storage systems by altering grain size, coating, or compounding with other materials. Xu et al. [19] evaluated the sand size to gain the optimum thermal storage. Then, they employed numerical and experimental investigation to increase the heat transfer inside their samples by adding Xceltherm (synthetic oil) and Hitec (inorganic salts). They exhibited that the grain size between 0.6 and 1.7 mm with a porosity of 0.38 is the suitable size distribution. They also found that if Hitec-saturated sand is utilized for storage media, energy can be stored more than Xceltherm, almost 35%. The findings show that new approaches developed under sensible heat storage can be significant in solar energy storage applications. García-Plaza et al. [24] prepared some sand coating utilizing a top-concentrated irradiation lamp in fluidized bed conditions. They found that graphite and carbon coats enhance the raw sand energy absorption between 30 and 40% due to higher thermal absorptivity. While the coats demonstrated constant properties after ten charging and discharging cycles, the color of graphite-coated sand faded from dark black to grey.

Sand is also used to mix with PCM materials. Barbi et al. [25] mixed N-octadence and commercial PCM (RT28) with sand in a ratio of 30% v/v separately to analyze their distribution in latent heat thermal energy storage for shallow geothermal applications. The results indicate that the heat transfer accelerated in both mixtures, halving the phase change time. In addition, sand addition led to a limited supercooling up to 1 °C in N-octadence. However, the phenomenon was absent in commercial PCM. In a related paper, Liu et al. [26] conducted some investigations into the thermal properties of recycled rubber-sand mixture via thermal needle tests. The study examined the impacts of various factors on thermal conductivity, including moisture proportion, moisture fraction, sand share, dry density, and particle size. The study proved that a higher proportion of sand increased the thermal conductivity of mixtures.

Tetteh et al. [27] analyzed experimentally and numerically different correlations for effective thermal conductivity of sand in a thermal storage application. Also, they utilized metallic chip layers to enhance the thermal conductivity of sand. The findings illustrated that a maximum heat rate is achievable when 20% of the volumetric amount of aluminum chips is mixed with sand. Moreover, Chung et al. [28] illustrated a practical method to run low-cost sand into a TES material and direct solar absorption through a thin silica shell and black spinel nanoparticles. The data revealed that the black quartz of sand incremented the solar absorbing rate almost two times, reaching ~0.89. The prototype also demonstrated a nearly unchanged stability of optical properties after 100 h at 800 °C. Analyzing the thermal conductivity of coated sand indicates an improvement from 0.30 (W/m/K) to 0.65 (W/m/K) from 20 °C to 700 °C. A comprehensive study was conducted by Palacios et al. [29]. They compared silicon carbide (Sic), silica sand (SiO_2), and hematite (Fe_2O_3) in terms of solar absorbing and specific heat capacity at different temperatures ranging from 750 to 900 °C. The experiment showed that hematite and silicon carbide significantly improved solar absorbance during the aging procedures. Reversely, silica sand reduced its absorbance over 100 h. After aging, the specific heat capacity indicator is ramped up in silicon carbide and silica sand samples. Reversly, iron oxide demonstrated a decline the specific heat capacity over the aging period. Due to its higher solar absorbance and heat storage capacity, the authors proved that black silicon carbide is the proper material for up to 900 °C.

Extensive sand extraction poses environmental challenges, prompting the need for alternative materials.[30, 31]. The recycled materials offer environmental benefits by reducing waste and present thermophysical properties suitable for TES applications. For instance, Al-Azawii et al. [32], conducted an experimental study on recycled ceramic material to use in a sensible heat-packed-bed thermal energy storage compared with A-alumina material. They applied an entire charging-discharging cycle with heat transfer fluid air at 150 °C. The findings indicated that the thermal charging process occurs faster in aluminum-based storage than in ceramic. Reversely, ceramic recorded a better performance in the discharging cycle. In another investigation, Py et al. [33] also used recycled industrial ceramics, vitrified asbestos-containing wastes, as sensible thermal storage material. The selected ceramic contains acceptable thermophysical properties for TES applications ($\lambda = 1.4$ W m/K, $Cp = 1025$ J kg/K, $\rho = 3100$ kg/m^3). The result verified that ceramic can be used as a thermal energy storage material for all types of concentrated solar power plants with operation levels of medium up to high concentration.

While there are several articles aimed at studying the thermophysical properties of sand and recycled materials for storage at high temperatures, there is limited literature for

civil and residential applications where the temperatures of interest are lower (40–80 °C). Although there are more efficient alternative solutions and materials for TES in residential applications (i.e. PCM material), using recycled ceramic materials becomes increasingly interesting due to the lower costs, even for poor societies. Previous studies, such as those by Kenda et al. [34], Calvet et al. [35], and Koçak et al. [36], have investigated certain waste materials concerning TES and thermophysical properties. However, their research primarily concentrated on specific materials and particular size ranges. Since the thermal behavior of granular materials is influenced by their size distribution, it becomes challenging to directly compare their findings. Therefore, a study is necessary to prepare the most common waste construction materials within the same size and an identical thermal analyzing process. The present study seeks to fill this research gap and also introduce an appropriate substitute for natural sand for thermal storage applications. The research examines the chemical properties, absolute density, specific heat capacity, thermal conductivity, and performance of the recycled materials in a one-cycle charging process. The results, illustrated in Ragone plots, aim to identify suitable recycled materials for thermal storage applications like water heating.

Methodology

In this investigation, experimental methods are employed to evaluate material properties relevant to the objectives of the present study, with subsequent numerical validation of the results. The process is depicted in Graph 1, starting with material crushing and terminating with the analysis of thermal storage behavior. Various techniques, including X-ray, hot disk, heat flow meter, and pycnometer methods, are utilized to assess chemical properties, specific heat capacity, thermal conductivity, and absolute density. The materials are dried at 105 °C. and tested under identical conditions, temperature and humidity. To ensure clarity and coherence, each experimental process and its corresponding result discussion are presented within the same section. In the end, the material's performances are demonstrated in Ragone plots regarding the material mass and volume (Fig. 1).

Experimental setups

Material collection and sieving

The materials were sourced from different sectors:

- Sand, a fine natural granular material.
- Glass, collected from urban waste, an equal share of clear and green bottles (50% of each).
- Ceramic, cooked tiles with a thin layer of glaze sourced from building demolition sectors.
- Concrete, gathered from the railway sleeper.
- Asphalt, obtained from crushed roads, has a bitumen proportion of 4.8%.

Sieving the natural sand revealed that the main proportion of grains is between 0.25 and 0.5 mm, about 40%, with the remaining share classified between 0.063 and 0.25 mm and 0.5 to 1 mm, around 30% each. This sizing distribution was applied to all recycled materials (Fig. 2). Meanwhile, the porosity of materials is 35%, according to the selected size and distribution. Before crushing and sieving, the materials were cleaned of any possible irrelevant ingredients, such as paper and plastics.

Chemical analysis

The materials underwent XRF analysis using a TESCAN MIRA3 to determine their chemical properties [37–39]. Each element has a specific emission of X-rays at specific energy levels, acting as unique fingerprints for that element. When the X-ray beam excites the sample's atoms, the instrument picks up the unique X-rays they emit [40, 41]. The instrument can identify each sample component by analyzing the spectrum's power and intensity [42, 43]. A carbon film was mounted onto suitable holders to set up this test, and the materials were stuck on the carbon layer [42]. A

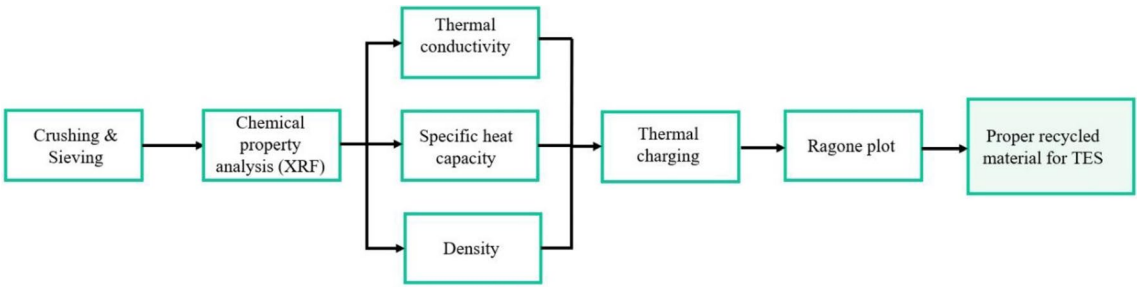

Fig. 1 Methodology process overview, detailing the sequential steps from material collection to thermal storage analysis

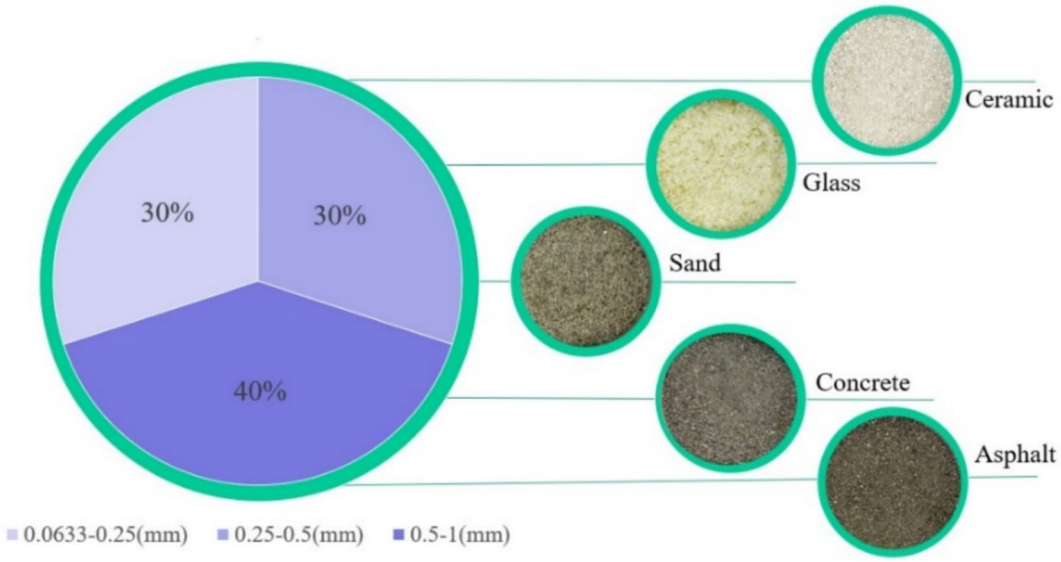

Fig. 2 Material size distribution of sand, ceramic, glass, concrete, and asphalt after sieving and preparation

vacuum chamber is deployed to keep samples in a proper condition to improve the electron beam stability and gain accurate results. The materials were evaluated for homogeneous patterns, and secondary detectors were used to gain deeper insight into the surface morphology and microstructure, ensuring the uniformity of structure and compounds.

The results indicate that 50% of the materials were composed of oxygen instead of concrete, which recorded the highest percentage (52.72%). Unlike sand and glass, which are rich in silicon dioxide, comprising 29% and 24%, respectively, ceramic is unique among the materials studied because it has a significantly higher aluminum content of 15.37%. Asphalt has a high level of carbon (31.07%) with small amounts of sulfur (1.04%) and magnesium (0.98%) which are either negligible or absent in the rest. Glass also has sodium(9.08%) and calcium(6.19%). The presence of a high quantity of calcium distinguishes concrete due to its structural properties, which must be noted (30.6%) (Fig. 3, Table 1).

Density analyzes

The density analysis was conducted using the pycnometer method under ASTM D5550–Standard [44–46]. In this test, two pycnometers are utilized to get the average result of the materials. The pycnometers were filled with pure water to begin the test, and their temperature and weight were recorded. Then, empty the pycnometer, completely dry their water and refill them again with a portion of the materials. After recording the net weight of materials, the pycnometer is filled partially until the sand sinks into the water. After that, the pycnometers are placed inside the suction machine with a vibration system for 15 min to release the air bubbles inside the material grains. Finally, the pycnometers were filled with water again, put in their caps, and weighed the total weight of materials, water, and pycnometer, refer to Fig. 4.

The collected data are imported into these equations to calculate the materials' absolute density.

$$V_m = \frac{(W_1 + W_2) - W_3}{\rho_w} \tag{1}$$

$$\rho_m = \frac{W_2}{V_m} \tag{2}$$

where:

- ρ_m = density of material (g/cm^3)
- ρ_w = density of water based on temperature (g/cm^3)
- V_m = volume of material (cm^3)
- W_1 = weight of pycnometer and water (g)
- W_2 = weight of material (g)
- W_3 = weight of pycnometer, material and water (g)

The density test illustrated that natural sand is the heaviest material, with 2.662 g/cm^3, followed by concrete, with 2.480 g/cm^3. Asphalt picks up the third level of heaviest material with 2.436 g/cm^3 and glass demonstrated a density of 2.421 g/cm^3. The lightest figure accounted for ceramic 2.285 g/cm^3 (Table 2).

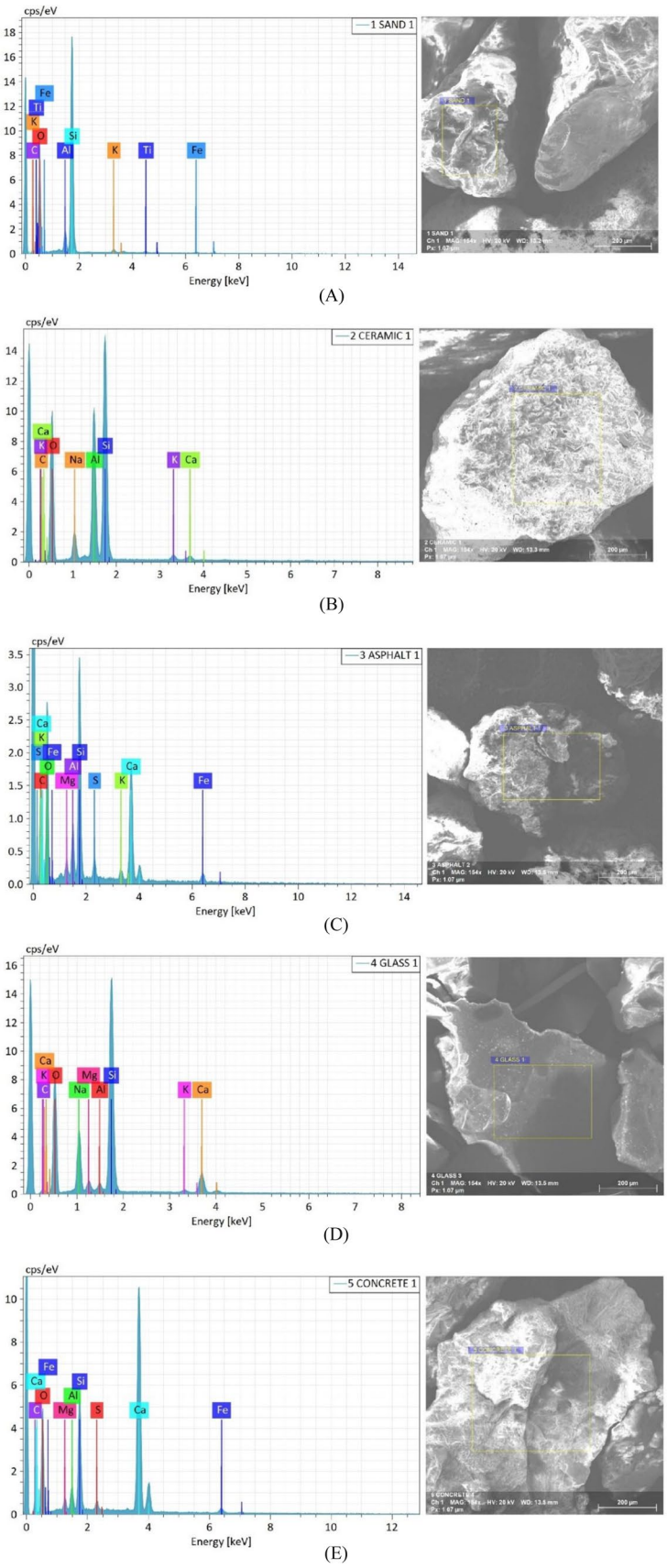

Fig. 3 Chemical composition analysis results for sand (**A**), ceramic (**B**), asphalt (**C**), glass (**D**), and concrete (**E**), including atomic percentage breakdowns

Table 1 Summary of chemical properties of sand, ceramic, asphalt, glass, and concrete, highlighting key elemental compositions

Chemical properties	Sand (%)	Ceramic (%)	Asphalt (%)	Glass (%)	Concrete (%)
C	8.36	3.37	31.07	6.43	5.99
O	57.4	51.43	45.88	51.46	52.72
Al	2.79	15.37	2.31	0.92	1.44
Si	29	24.09	7.86	24.01	6.15
K	0.86	0.98	0.58	0.61	0
Ti	0.74	0	0	0	0
Fe	0.85	0	1.29	0	1.53
Na	0	3.78	0	9.08	0
Ca	0	0.97	8.99	6.19	30.6
Mg	0	0	0.98	1.31	0.83
S	0	0	1.04	0	0.74

Thermal conductivity analysis

Thermal conductivity analysis, based on the heat flow meter method, allows for determining the steady-state thermal conductivity of materials with $\lambda < 5$ (W/mK) [47–50]. This apparatus has been designed under the principle of ISO 9301 [51]. Two heat flow meters are utilized with a single-specimen symmetrical configuration, and a helical counter-flow path is fed to the hot and cold plates with a liquid (Fig. 5). The temperature of the plates is controlled by two thermostatic baths, having temperatures ranging between − 15 and + 90 °C. The working plate of heating and cooling units is realized with copper smoothly conformed to a proper plane within 0.02%. An IR Thermo-camera was used to evaluate the temperature uniformity of both working surfaces, as the temperature nonuniformity should be less than 1% of temperature differences across the specimen indicated by ISO 8301 [52–55]. Several temperature sensors are connected to the surface of the metering area measuring 25 cm × 25 cm. However, the sample size is considered 30 × 30 × 4.2 cm in this Study. The system calculates the thermal conductivity under this equation:

$$\lambda = fe\frac{d}{\Delta T} \tag{3}$$

where;

- d = Average specimen thickness (m)

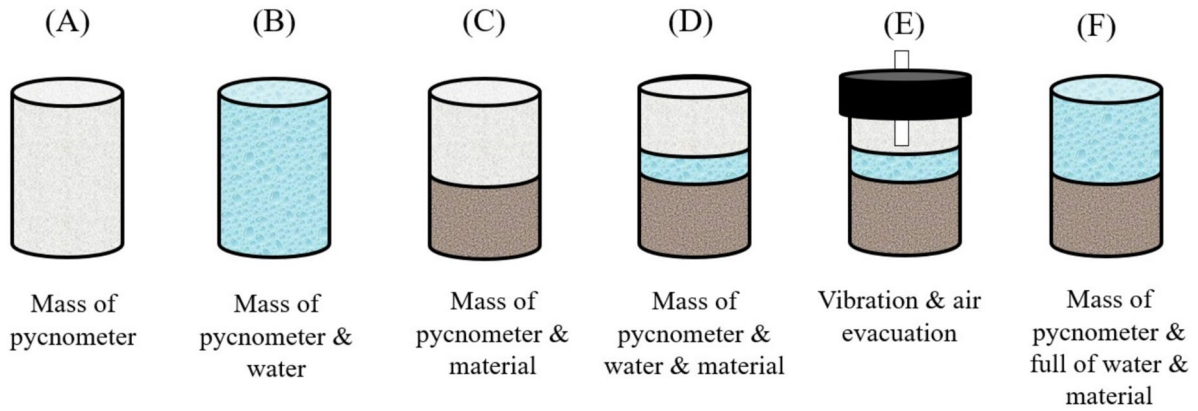

Fig. 4 Workflow of the absolute density analysis process using the pycnometer method

Table 2 Absolute density results for sand, ceramic, asphalt, glass, and concrete, obtained using the pycnometer method

Particulars	Sand		Glass		Concrete		Asphalt		Ceramic	
Pycnometer No	1	2	1	2	1	2	1	2	1	2
Temperature of water (°C)	18	18	17	17	17	17	18	18	17	17
W_4 (g)	1881.35	1873.58	1881.76	1873.48	1881.76	1873.48	1881.35	1873.58	1881.76	1873.48
W_5 (g)	550.01	550.76	501.59	500.94	500.24	500.71	501.3	500.91	500.81	500.26
W_3 (g)	2225.02	2217.79	2176.33	2167.89	2180.62	2172.47	2177.01	2169.31	2162.82	2155.86
ρ_w (g/cm^3)	0.99862	0.99862	0.9988	0.9988	0.9988	0.9988	0.99862	0.99862	0.9988	0.9988
V_m (cm^3)	206.625	206.835	207.269	206.778	201.622	201.962	205.924	205.464	220.014	218.142
ρ_m (g/cm^3)	2.66187	2.66279	2.42	2.4226	2.48108	2.47922	2.43439	2.43795	2.27626	2.29328
Average density of material (g/cm^3)	2.662		2.421		2.480		2.436		2.285	

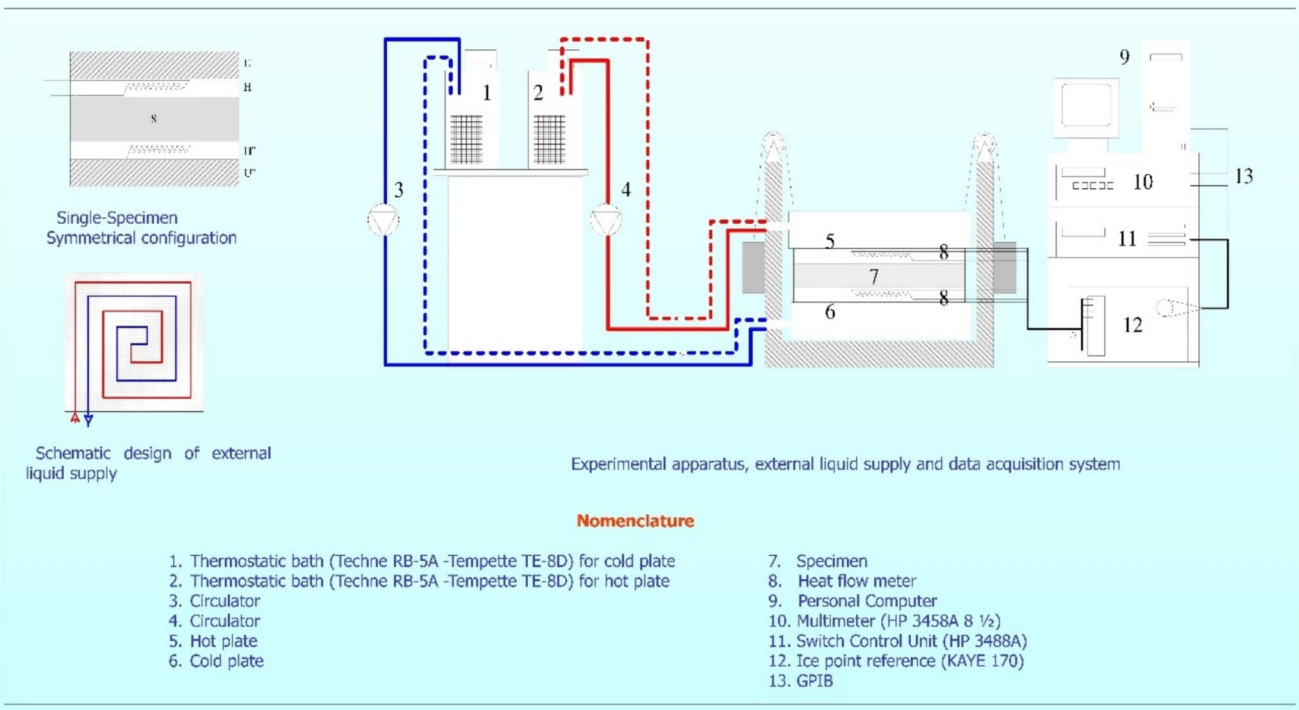

Fig. 5 Experimental setup of the heat flow meter for thermal conductivity analysis, showing critical components and measurement configuration

- f = calibration factor of the heat flow meter (W/mV m^2)
- e = heat flow meter output (mV)
- ΔT = temperature difference (C)

The samples were tested for 24 h at an identical initial temperature and humidity. The results indicate that natural sand has the highest thermal conductivity, with 0.189 (W/mK), and concrete recorded the second highest by 0.172 (W/mK). The lowest thermal conductivity figure registered by the glass was 0.131 (W/mK). In addition, Fig. 6 explicates that ceramic and asphalt recorded 0.159 and 0.152 (W/mK), respectively.

Specific heat capacity

A hot disk instrument is employed to evaluate the materials' specific heat capacity, which is crucial when calculating thermal capacity. The instrument uses the Transient Plane Source (TPS) method. This method, which determines solid materials' thermal conductivity and thermal diffusivity, is pivotal to the instrument's accuracy [56]. This method fills the materials inside a thermal conductive container capsulated with thermal insulation to prevent any energy release during the test. The sample container was made of copper, which measured R = 10 mm and H = 4 mm. The metal container, linked to a fixed power source and a hot disk sensor, is vital for the measurement process (see Fig. 7). Both power and time are essential parameters in this analysis. However,

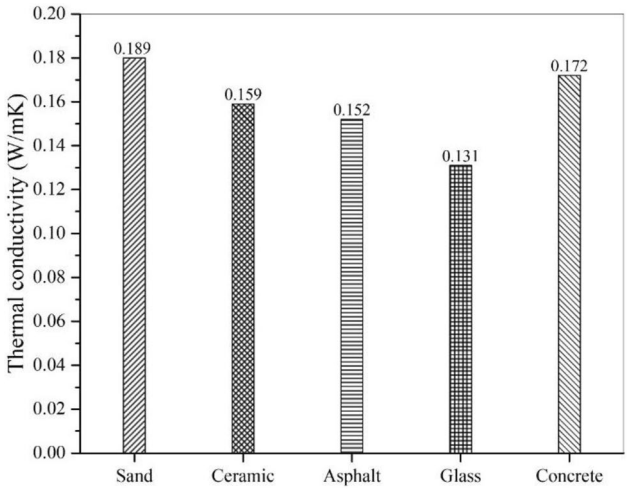

Fig. 6 Thermal conductivity values of sand, ceramic, asphalt, glass, and concrete under identical testing conditions

establishing steady temperature gradients within the container and the material sample over time is paramount. This ensures accurate and reliable results. The sensor's temperature, which increases continuously, is monitored by tracking the corresponding rise in its electrical resistance.[57]. Before initiating the Hot Disk setup, the empty metallic container was powered with 100 mW for 80 s at 23 °C to obtain reference data. Then, the solid material sample was balanced, positioned inside the enclosure, and protected on the sample

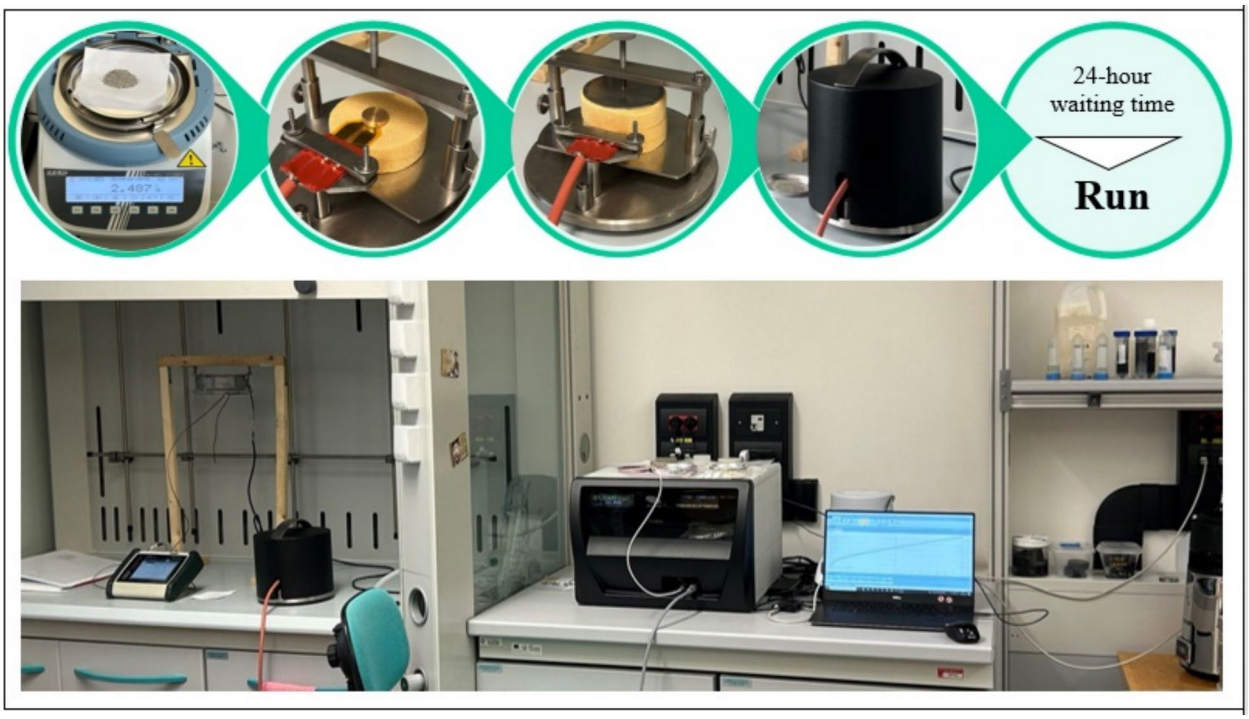

Fig. 7 Hot disk instrument setup for determining specific heat capacity, detailing the test parameters and materials used

holder. The container and sample holder were covered with a black metal shield to reduce the impact of air currents on the device's performance. The experimental setup was operated one day after each sample was placed in its designated position, ensuring consistency in the analysis conditions. These conditions mirrored those used for the reference measurement with the empty metallic container.

The results of the Hot Disk analysis demonstrated that concrete recorded the most outstanding figure, with 755 (J/kg K) emerging as a proper choice for extensive heat storage and gradual release compared to other materials. Asphalt accounted for the second-highest specific heat capacity with 732 J/kg K, about six percent lower than concrete (Fig. 8). Glass, with a specific heat capacity of 708 J/kg K delivers a moderate performance. On the contrary, sand and ceramic demonstrated lower specific heat capacities of 688 J/kg K and 682 J/kg K, respectively.

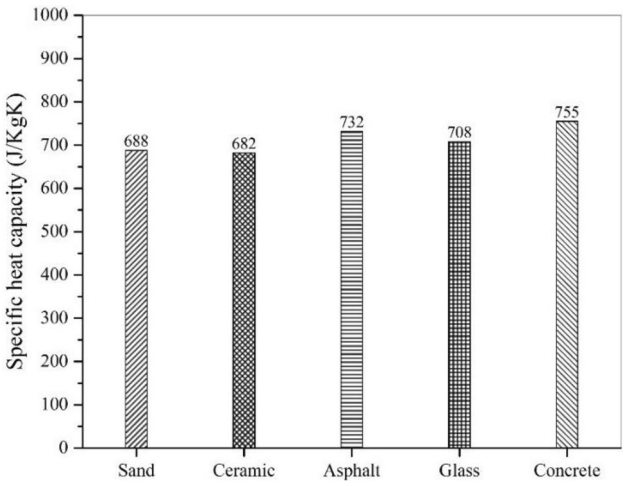

Fig. 8 Specific heat capacity results for sand, ceramic, asphalt, glass, and concrete, highlighting differences in thermal storage capacity

Thermal charging test

This experiment aims to assess the thermal behavior of materials during heat absorption. Regarding residential applications like water heating, the suitable water temperature ranges between 55 65 and 70 °C. Therefore, experimental measurements were performed to reach a mean value of 60 °C of the material under test.

Identical experimental conditions were designed for all specimens to ensure accurate comparisons. Tin-coated steel containers were colored black to maximize heat absorption. The container volume is 427.5 cm^3, measuring R = 4.075 cm, H = 8.2 cm. In addition, A Type T thermocouple was placed in the center of each container to record the material temperature.

The prepared materials were filled into the metal containers and subjected to a shaker device for 3 min at 150 rpm to achieve uniform bulk density. The obtained densities are sand 1672 kg (m: 0.715), ceramic 1377 kg (m:

0.589), asphalt 1480 kg (m: 0.633), glass 1426 kg (m: 0.610), and concrete 1546 kg (m: 0.661). The top surface of each container was covered with a thin layer of black plastic to minimize the influence of the material's color on the endothermic process. A radiation technique was deployed instead of a direct heating source to design a similar heat transfer in an outdoor environment. Thus, a 42-W lamp is utilized and fixed inside a plastic enclosure to prevent air velocity interference. An additional thermocouple was placed in plastic containers to record air temperature during the charging- period (Fig. 9).

Following the material preparation, the metal container was positioned in the center of the plastic enclosure, with the lamp placed 3 cm above the sample's top surface. The thermocouples were connected to a data collector, transferring the temperature data to a laptop. The initial temperature of the samples was set at 26.5°C, matching the room temperature. The experiment was conducted over six hours.

Figure 10 shows the ambient air temperature produced by the lamp increased rapidly from 26.5 to 55 °C after 120 min. Then, it recorded a smooth rise, reaching almost 60 °C over the charging cycle. Concerning the internal temperature of the samples, ceramic and sand recorded the highest temperature in the heating process, 59 °C, followed by glass at 57.89 °C. Concrete and sand stayed at a lower internal temperature of 57.60 and 57.03 °C, respectively.

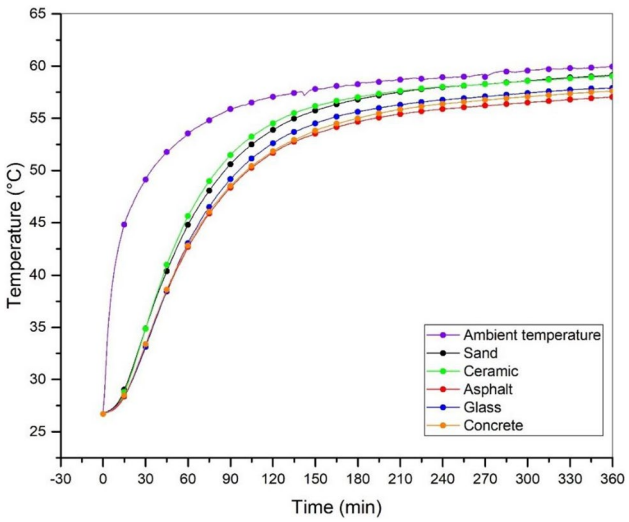

Fig. 10 Temperature profiles of sand, ceramic, asphalt, glass, and concrete over a six-hour charging cycle

Thermal storage capability

Drawing the Ragone plot can demonstrate the materials' thermal storage behavior, and in this sense, Woods et al. [58] utilized it to evaluate the thermal storage capability of PCM at different thicknesses and to supply power. In addition, [59] Lin et al. employed Ragone plots in designing thermal batteries based on phase change materials. Therefore, the

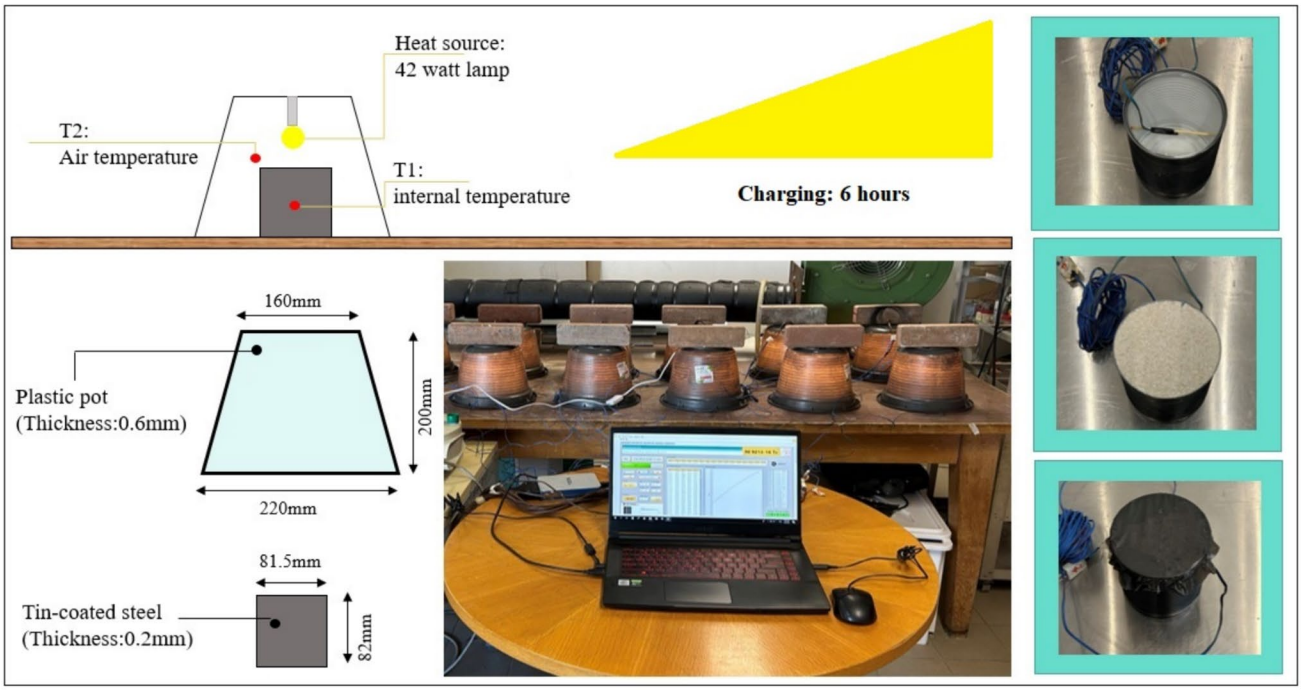

Fig. 9 Experimental setup for thermal charging tests, demonstrating material placement, heat source, and temperature monitoring system

Ragone plot compares the materials' thermal storage performance. The recorded data in the charging cycle experiment is transferred into two Ragone Plots based on the following equations [60–62], and the results are represented in Table 3.

$$\text{Specific energy and power}\begin{cases} u_s = \frac{E}{m} = \frac{m \times Cp \times \Delta T}{m} = Cp \times \Delta T \quad (4) \\ p_s = \frac{P}{m} = \left(\frac{E}{t}\right)/m \quad (5) \end{cases}$$

$$\text{Volumetric energy and power density}\begin{cases} u_v = \frac{E}{V} = \frac{m \times Cp \times \Delta T}{V} \quad (6) \\ p_v = \frac{P}{V} = \left(\frac{E}{t}\right)/V \quad (7) \end{cases}$$

where;

- u_s = specific energy (J/kg)
- u_v = volumetric energy density (J/m^3)
- E = total energy stored (J)
- V = volume (m^3)
- m = mass (kg)
- cp = specific heat capacity (J/kg·°C)
- ΔT = change in temperature (°C)

And,

- p_s = specific power (W/kg)
- p_v = *volumetric power density (W/m^3)*
- P = power output (W)
- t = time (s)

The first Ragone plot (Fig. 11) indicates specific power (W/kg) against specific energy (J/kg) for successive 30-min intervals. Specific power is an indicator of the power output per unit mass. Reversely, specific energy demonstrates the energy stored per unit mass. These metrics are pivotal for applications where weight is a significant constraint. Initially, all materials depict an upward trend in power output. However, ceramic recorded a rapid growth, reaching the highest peak specific power of around 3.6 W/kg at approximately 1.3×10^4 J/kg. This high specific power makes ceramic ideal for solar applications where rapid energy release is essential. Then, it demonstrated a remarkable reduction, indicating a rapid decline in efficiency at higher energy density. Sand, asphalt, and glass recorded around 3.53 W/kg, 3.33 W/kg, and 3.3 W/kg, respectively, at approximately 1.2×10^4 J/kg before declining, though sand's efficiency also declines significantly at higher energy densities. Concrete peaks at around 3.48 W/kg at about 1.2×10^4 J/kg. It also retains a relatively high specific power over a broader range of specific energies. This shows that concrete

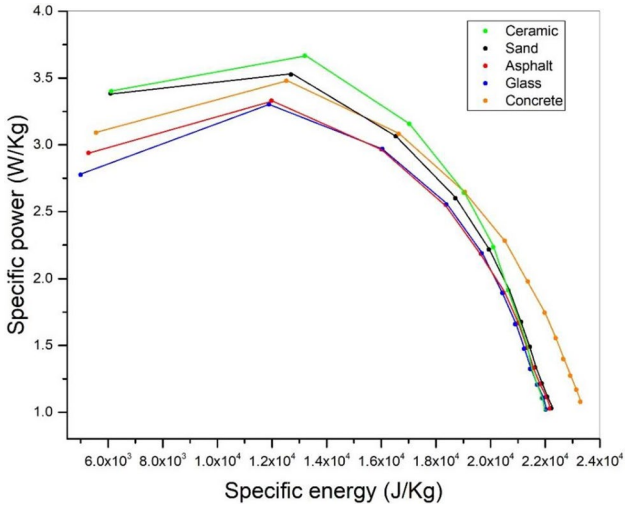

Fig. 11 Ragone plot showing the relationship between specific energy and specific power for sand, ceramic, asphalt, glass, and concrete

Table 3 Specific energy (J/kg) and specif power (W/kg) data for all materials over 30-min intervals, derived from the charging test results

Time	Sand		Ceramic		Asphalt		Glass		Concrete	
	p_s	e_s	p_s	e_s	p_s	e_s	p_s	e_s	p_s	e_s
30′	3.38	6089	3.40	6120	2.94	5288	2.78	4996	3.09	5562
60′	3.53	12,693	3.67	13,198	3.33	11,983	3.30	11,890	3.48	12,523
90′	3.06	16,537	3.15	17,036	2.97	16,012	2.97	16,036	3.08	16,640
120′	2.60	18,714	2.64	19,017	2.55	18,362	2.55	18,380	2.65	19,057
150′	2.22	19,937	2.23	20,095	2.18	19,651	2.19	19,683	2.28	20,520
180′	1.91	20,648	1.91	20,661	1.90	20,467	1.89	20,438	1.98	21,369
210′	1.68	21,121	1.67	21,049	1.67	20,996	1.66	20,894	1.74	21,985
240′	1.49	21,434	1.48	21,318	1.48	21,336	1.47	21,226	1.55	22,382
270′	1.34	21,629	1.33	21,486	1.33	21,568	1.32	21,451	1.40	22,657
300′	1.22	21,871	1.21	21,703	1.21	21,801	1.21	21,709	1.27	22,912
330′	1.11	22,073	1.10	21,873	1.11	22,002	1.11	21,906	1.17	23,132
360′	1.03	22,221	1.02	22,017	1.03	22,165	1.02	22,018	1.08	23,291

has a good energy storage capability for specific power over a wider range of specific energies (Table 3).

The second Ragone plot depicts the relation between volumetric power density (W/m^3) and volumetric energy density (J/m^3). Volumetric power and energy density indicate the power output and energy stored per unit volume. These indicators are particularly crucial for applications where space constraint exists, such as in urban infrastructure and compact energy storage systems. According to Fig. 12 and Table 4, sand accounted for the highest peak volumetric power density, approximately at 5896 W/m^3, with a volumetric energy of 2.1 × 107. This performance shows that it can distribute notable power output regarding the volume, and it is reminded of higher volumetric power density over time compared with other materials. Concrete, on the other hand, recorded the second-highest power density with a peak point of 5378 W/m^3. Asphalt and glass illustrated the same trend of up and downward movements with a peak volumetric power of 4928 W/m^3 and 4712 W/m^3.

In contrast, ceramic slightly increased slightly from 4684 to 5051 W/m^3. Then, it recorded a sharp post-peak decline. Figure 12 Ragone plot for specific energy and power [58, 59, 63].

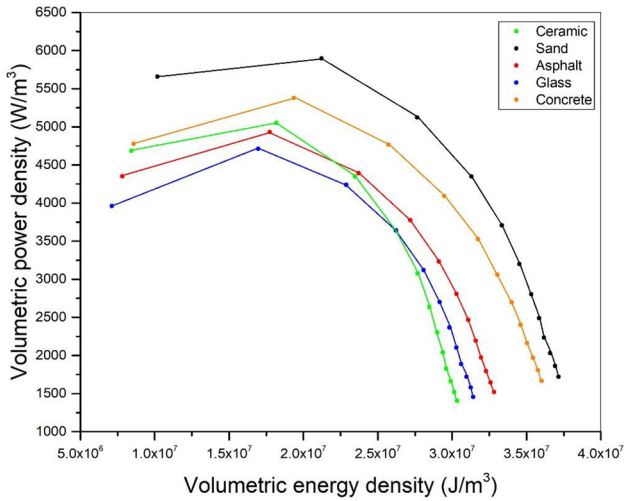

Fig. 12 Ragone plot depicting volumetric energy density and power density for sand, ceramic, asphalt, glass, and concrete

Conclusion

Thermal energy storage has gained importance in energy conservation since it is adaptable to various renewable energy sources. Solar and wind power highly depend on weather conditions day and night. Therefore, thermal storage systems can store the available energy in appropriate weather conditions and send it to the building supplying system. Generally, three thermal storage materials are in the physical state, including phase-change, liquid, and solid materials. In recent decades, granular materials like sand have gained attention due to cycle stability and low cost in providing and maintaining; however, excessive use of natural sand has incurred environmental issues. Reversely, recycled construction materials such as concrete can be a reliable substitute for natural sand in thermal storage and solar concentrator applications. Thus, construction waste materials can be reproduced instead of disposed of in landfills. This study evaluated the thermal storage capability of four recycled materials for low-temperature applications, comprising glass, asphalt, ceramic, and concrete. The findings demonstrate that recycled concrete can be a reliable alternative to natural sand in TES systems due to its higher specific heat capacity and lower thermal conductivity. Reversely, ceramic illustrated a fast temperature increase in the thermal charging process, specifically in the first 30 min, indicating a greater

Table 4 Volumetric energy (J/m^3) and power density (W/m^3) measurements for sand, ceramic, asphalt, glass, and concrete, emphasizing differences in thermal storage efficiency

Time	Sand		Ceramic		Asphalt		Glass		Concrete	
	p_v	u_v	p_v	u_v	p_v	u_v	p_v	u_v	p_v	u_v
30′	5658	10,184,633	4684	8,432,083	4350	7,830,240	3961	7,129,347	4777	8,599,431
60′	5897	21,228,620	5051	18,184,597	4929	17,743,237	4713	16,966,354	5379	19,363,215
90′	5122	27,658,858	4347	23,471,263	4391	23,708,873	4237	22,882,230	4765	25,729,142
120′	4347	31,298,941	3639	26,201,586	3776	27,188,309	3643	26,226,466	4093	29,466,186
150′	3705	33,344,627	3076	27,686,504	3233	29,096,763	3121	28,085,635	3525	31,728,227
180′	3198	34,533,423	2636	28,465,978	2806	30,305,279	2700	29,162,588	3059	33,040,687
210′	2804	35,325,838	2302	29,000,491	2467	31,088,134	2366	29,813,145	2698	33,993,057
240′	2490	35,849,191	2040	29,371,906	2194	31,591,965	2103	30,287,643	2403	34,606,882
270′	2233	36,175,640	1827	29,603,115	1971	31,936,100	1889	30,609,116	2162	35,032,407
300′	2032	36,579,873	1661	29,901,344	1793	32,280,545	1721	30,976,099	1968	35,426,701
330′	1864	36,916,981	1522	30,136,306	1645	32,577,989	1579	31,257,846	1806	35,767,273
360′	1721	37,164,695	1404	30,334,971	1519	32,819,905	1454	31,416,818	1667	36,012,752

heat transfer rate, which is suitable to mix with PCMs to reduce their melting and solidification times. Future studies should focus on optimizing concrete thermal properties by using admixtures and treatments that can improve its efficiency. Recycled concrete can provide durable and low-cost thermal energy storage that can be utilized for water heating in unprivileged communities.

Declarations

Conflict of interest On behalf of all authors, the corresponding author states that there is no conflict of interest.

References

1. Kebede, A.A., et al.: A comprehensive review of stationary energy storage devices for large scale renewable energy sources grid integration. Renew. Sustain. Energy Rev. **159**, 112213 (2022)
2. Ahmad, A., et al.: A comprehensive material and experimental investigation of a packed bed latent heat storage system based on waste foundry sand. Energy **294**, 130920 (2024)
3. Mitali, J., Dhinakaran, S., Mohamad, A.: Energy storage systems: a review. Energy Storage Sav. **1**(3), 166–216 (2022)
4. Chen, T., et al.: Applications of lithium-ion batteries in grid-scale energy storage systems. Trans. Tianjin Univ. **26**(3), 208–217 (2020)
5. Olivetti, E.A., et al.: Lithium-ion battery supply chain considerations: analysis of potential bottlenecks in critical metals. Joule **1**(2), 229–243 (2017)
6. Doucette, R.T., McCulloch, M.D.: A comparison of high-speed flywheels, batteries, and ultracapacitors on the bases of cost and fuel economy as the energy storage system in a fuel cell based hybrid electric vehicle. J. Power. Sources **196**(3), 1163–1170 (2011)
7. Chen, H., et al.: Progress in electrical energy storage system: a critical review. Prog. Nat. Sci. **19**(3), 291–312 (2009)
8. Lu, C., et al.: Optimal sizing and control of battery energy storage system for peak load shaving. Energies **7**(12), 8396–8410 (2014)
9. Zhao, B., Ding, Y., Wen, Z.: From jackfruit rags to hierarchical porous N-doped carbon: a high-performance anode material for sodium-ion batteries. Trans. Tianjin Univ. **25**, 429–436 (2019)
10. Nikolina, S.: International renewable energy agency (IRENA) (2016)
11. Sarbu, I., Sebarchievici, C.: A comprehensive review of thermal energy storage. Sustainability **10**(1), 191 (2018)
12. Sarbu, I., Sebarchievici, C.: Solar Heating and Cooling Systems: Fundamentals, Experiments and Applications. Elsevier, Oxford (2016)
13. Makhanya, N., et al.: Recent advances on thermal energy storage using metal-organic frameworks (MOFs). J. Energy Storage **34**, 102179 (2021)
14. Suresh, C., Saini, R.P.: Review on solar thermal energy storage technologies and their geometrical configurations. Int. J. Energy Res. **44**(6), 4163–4195 (2020)
15. Sharma, A., et al.: Review on thermal energy storage with phase change materials and applications. Renew. Sustain. Energy Rev. **13**(2), 318–345 (2009)
16. Rohit, A.K., Rangnekar, S.: An overview of energy storage and its importance in Indian renewable energy sector: Part II–energy storage applications, benefits and market potential. J. Energy Storage **13**, 447–456 (2017)
17. Desai, N., Haglind, F.: Concentrated Solar Energy Driven Multi-generation Systems Based on the Organic Rankine Cycle Technology, in Advances in Carbon Management Technologies. Taylor & Francis, Milton Park (2020)
18. Li, X., et al.: Experimental investigation and thermodynamic modeling of an innovative molten salt for thermal energy storage (TES). Appl. Energy **212**, 516–526 (2018)
19. Xu, B., et al.: Thermal storage using sand saturated by thermal-conductive fluid and comparison with the use of concrete. J. Energy Storage **13**, 85–95 (2017)
20. Diago, M., et al.: Characterization of desert sand to be used as a high-temperature thermal energy storage medium in particle solar receiver technology. Appl. Energy **216**, 402–413 (2018)
21. Li, M., Zhou, D., Jiang, Y.: Preparation and thermal storage performance of phase change ceramsite sand and thermal storage light-weight concrete. Renew. Energy **175**, 143–152 (2021)
22. Warerkar, S., et al.: Air-sand heat exchanger for high-temperature storage (2011)
23. Kiwan, S., Soud, Q.R.: Experimental investigation of the thermal performance of a sand-basalt heat storage system for beam-down solar concentrators. Case Stud. Therm. Eng. **19**, 100609 (2020)
24. García-Plaza, J., et al.: Experimental study of different coatings on silica sand in a directly irradiated fluidised bed: thermal behaviour and cycling analysis. Appl. Therm. Eng. **217**, 119169 (2022)
25. Barbi, S., et al.: Phase change material-sand mixtures for distributed latent heat thermal energy storage: interaction and performance analysis. Renew. Energy **169**, 1066–1076 (2021)
26. Liu, L., Cai, G., Liu, X.: Investigation of thermal conductivity and prediction model of recycled tire rubber-sand mixtures as lightweight backfill. Constr. Build. Mater. **248**, 118657 (2020)
27. Tetteh, S., et al.: Improved effective thermal conductivity of sand bed in thermal energy storage systems. J. Energy Storage **86**, 111350 (2024)
28. Chung, K.M., Chen, R.: Black coating of quartz sand towards low-cost solar-absorbing and thermal energy storage material for concentrating solar power. Sol. Energy **249**, 98–106 (2023)
29. Palacios, A., et al.: Study on solar absorptance and thermal stability of solid particles materials used as TES at high temperature on different aging stages for CSP applications. Sol. Energy Mater. Sol. Cells **201**, 110088 (2019)
30. Diago, M., et al.: Characterization of desert sand for its feasible use as thermal energy storage medium. Energy Procedia **75**, 2113–2118 (2015)
31. Martinkauppi, J., et al.: Some aspects of recycling concrete crush for thermal heat storage. In: 2018 7th International Conference on Renewable Energy Research and Applications (ICRERA). IEEE (2018)
32. Al-Azawii, M.M., et al.: Experimental study on packed-bed thermal energy storage using recycled ceramic as filler materials. J. Energy Storage **44**, 103375 (2021)
33. Py, X., et al.: Recycled material for sensible heat based thermal energy storage to be used in concentrated solar thermal power plants (2011)

34. Kenda, E.S., et al.: Thermal energy storage materials made of natural and recycled resources for CSP in West Africa. Waste Biomass Valoriz. **9**, 1687–1701 (2018)
35. Calvet, N., et al.: Waste from metallurgic industry: a sustainable high-temperature thermal energy storage material for concentrated solar power. In: Energy Sustainability. American Society of Mechanical Engineers (2013)
36. Koçak, B., Fernandez, A., Paksoy, H.: Benchmarking study of demolition wastes with different waste materials as sensible thermal energy storage. Sol. Energy Mater. Sol. Cells **219**, 110777 (2021)
37. Maestracci, B., et al.: Simultaneous combined XRF-XRD analysis of geological sample: new methodological approach for on-site analysis on New-Caledonian Ni-rich harzburgite. J. Geochem. Explor. **252**, 107250 (2023)
38. Klimko, J., Oráč, D., Klein, D.: Recycling of lithium accumulators. In: 2019 International Council on Technologies of Environmental Protection (ICTEP). IEEE (2019)
39. Pashkova, G.V., et al., Applicability of total reflection x-ray fluorescence for heavy metal analysis in Lake Baikal sponges. X-Ray Spectrom. (2023)
40. Wagner, J., et al.: Source identification on high PM2.5 days using SEM/EDS, XRF, Raman, and windblown dust modeling. Aerosol Air Qual Res **19**(11), 2578–2530 (2019)
41. Zizkova, N., et al.: Mortars with crystalline additive in aggressive environments. In: IOP Conference Series: Materials Science and Engineering. IOP Publishing (2018)
42. Amiri, A., Toufigh, M.M., Toufigh, V.: Recycling and utilization assessment of municipal solid waste materials to stabilize aeolian sand. KSCE J. Civ. Eng. **27**(3), 1042–1053 (2023)
43. Safonov, A., et al.: The microbial impact on U, Pu, Np, and Am immobilization on aquifer sandy rocks, collected at the deep LRW injection site. J. Geochem. Explor. **240**, 107052 (2022)
44. Flint, A.L., Flint, L.E.: 2.2 particle density. Methods of soil analysis: Part 4 physical methods **5**, 229–240 (2002)
45. Blake, G., Hartge, K.: Particle density. Methods of soil analysis: Part 1 physical and mineralogical methods **5**, 377–382 (1986)
46. Makhuvha, M., Arellano, R., Harney, D.: Determination of bulk density, methods and impacts, with a case study from Los Bronces Mine, Chile. Appl. Earth Sci. **123**(3), 196–205 (2014)
47. Haigh, S.: Thermal conductivity of sands. Geotechnique **62**(7), 617–625 (2012)
48. Alrtimi, A., Rouainia, M., Haigh, S.: Thermal conductivity of a sandy soil. Appl. Therm. Eng. **106**, 551–560 (2016)
49. Ruuska, T., Vinha, J., Kivioja, H.: Measuring thermal conductivity and specific heat capacity values of inhomogeneous materials with a heat flow meter apparatus. J. Build. Eng. **9**, 135–141 (2017)
50. Liu, K., et al.: An experimental study on thermal conductivity of iron ore sand cement mortar. Constr. Build. Mater. **101**, 932–941 (2015)
51. Yılmaz, F., et al.: Potential of aerobic membrane bioreactor for recycling and reuse of domestic wastewater for irrigation. Environ. Earth Sci. **79**, 1–11 (2020)
52. Łoziczonek, H.B., Furtak, M.: Methods of determining the thermal conductivity of building materials with high and medium thermal resistance. In: AIP Conference Proceedings. AIP Publishing (2023)
53. Aslan, M., Öztürk, H., Demirkır, C.: Investigation of thermal conductivity of wood Sandwich panels with Aluminium and polypropylene core. J. Anat. Environ. Anim. Sci. **4**(4), 647–650 (2019)
54. Fustinoni, D., et al.: Accurate contact resistance characterization for thermal conductivity measurement with the Heat Flow Meter method. J. Phys. Conf. Ser. (2021)
55. Koru, M.: Determination of thermal conductivity of closed-cell insulation materials that depend on temperature and density. Arab. J. Sci. Eng. **41**, 4337–4346 (2016)
56. Gustavsson, M., et al.: Specific heat measurements with the hot disk thermal constants analyser. In: Thermal Conductivity, vol. 23, pp. 56–65. CRC Press (2021)
57. Mydin, M.A.O.: Assessment of thermal conductivity, thermal diffusivity and specific heat capacity of lightweight aggregate foamed concrete. J. Teknol. Sci. Eng **78**(5), 477–482 (2016)
58. Woods, J., et al.: Rate capability and Ragone plots for phase change thermal energy storage. Nat. Energy **6**(3), 295–302 (2021)
59. Lin, X.-W., et al.: Rate capability and Ragone plots for designing battery thermal management system based on phase change material. J. Energy Storage **74**, 109539 (2023)
60. Sun, Y., et al.: A bamboo-inspired nanostructure design for flexible, foldable, and twistable energy storage devices. Nano Lett. **15**(6), 3899–3906 (2015)
61. Obeidat, A.M., Rastogi, A.: Co-electrodeposited poly (3, 4-ethylenedioxythiophene)(PEDOT)-multiwall carbon nanotubes (MWCNT) hybrid electrodes based solid-state supercapacitors using ionic liquid gel electrolyte for energy storage with pulsed power capabilities. J. Energy Storage **67**, 107563 (2023)
62. Gopi, C.V.M., et al.: Recent progress of advanced energy storage materials for flexible and wearable supercapacitor: From design and development to applications. J. Energy Storage **27**, 101035 (2020)
63. Allagui, A., Fouda, M.E., Elwakil, A.S.: Communication—the Ragone plot of supercapacitors under different loading conditions. J. Electrochem. Soc. **167**(2), 020533 (2020)